

A Physical Model for Seismic Noise Generation from Sediment Transport in Rivers

Victor C. Tsai^{1,2}, Brent Minchew^{1,2}, Michael P. Lamb², and Jean-Paul Ampuero^{1,2}

Measuring sediment flux in rivers remains a significant problem in studies of landscape evolution. Recent studies suggest that observations of seismic noise near rivers can help provide such measurements, but the lack of models linking observed seismic quantities to sediment flux has prevented the method from being used. Here, we develop a forward model to describe the seismic noise induced by the transport of sediment in rivers. The model provides an expression for the power spectral density (PSD) of the Rayleigh waves generated by impulsive impacts from saltating particles which scales linearly with the number of particles of a given size and the square of the linear momentum. After incorporating expressions for the impact velocity and rate of impacts for fluvially transported sediment, we observe that the seismic noise PSD is strongly dependent on the sediment size, such that good constraints on grain size distribution are needed for reliable estimates of sediment flux based on seismic noise observations. The model predictions for the PSD are consistent with recent measurements and, based on these data, a first attempt at inverting seismic noise for the sediment flux is provided.

1. Introduction

The transport of coarse sediment by rivers sets the pace of landscape evolution by controlling channel morphology and the rates of bedrock incision [e.g., Whipple, 2004]. Moreover, accurate predictions of sediment flux are needed for diverse applications including sedimentation engineering, river restoration, and flood hazard mitigation. Most models for bedload sediment transport are empirical and typically rely on data from flume experiments where sediment flux is at the transport capacity [e.g., Fernandez Luque and van Beek, 1976]. In many mountain streams, sediment flux is under-capacity, however, and is governed by the sediment supply from upstream and neighboring hillslopes, for which no bedload-flux models exist [e.g., Whipple, 2004]. Our inability to accurately model bedload transport stems from a lack of measurements during floods in steep rivers where traditional measurement techniques (e.g., sediment traps) are extremely difficult, if not impossible, to apply.

A potential solution to this data gap is to use acoustic or seismic energy from bedload particle impacts as a proxy for sediment flux [Govi *et al.*, 1993; Barton *et al.*, 2006; Burtin *et al.*, 2008; Hsu *et al.*, 2011]. High-frequency (> 1 Hz) seismic noise near rivers has been shown to correlate with river discharge [Burtin *et al.*, 2008, 2010, 2011; Hsu *et al.*, 2011], and the observed increase of seismic noise with increasing flow depth has, in all cases, been partly attributed to particles impacting bedrock. Burtin *et al.* [2010]

show that the majority of this seismic noise observed in Nepal is generated in reaches of the Trisuli River with high gradients. Similar to Burtin *et al.* [2008], Hsu *et al.* [2011] argue that observed hysteresis in high frequency seismic power relative to river discharge during major storms in Taiwan is related to sediment transport. However, none of the above mentioned studies were able to directly convert measurements of seismic noise into bedload flux because a theoretical underpinning that relates the two has yet to be developed.

Herein, we derive a simple analytical model for the seismic noise produced by impacting river sediment. We present preliminary model results using estimates of river and sediment parameters based on studies of Himalayan rivers [Lavé and Avouac, 2001; Attal and Lavé, 2006; Gabet *et al.*, 2008] in order to compare our results with measurements of Burtin *et al.* [2008].

2. Model

Our goal is to derive a mechanistic model for seismic noise generated by river sediment-bed impacts using as simple and generic of parameterizations as possible that still incorporate the relevant first-order physics. The primary idea of this model is that each sediment particle impacts the river bed and creates a force impulse that then excites seismic waves that travel to nearby seismic stations. With many particles, each impacting the bed at random times relative to the others, one can calculate the total noise power spectral density (PSD) observed at a given station. To attempt to make comparisons with the observations discussed in the Introduction, we make model predictions over the frequency range $1 \text{ Hz} < f < 1000 \text{ Hz}$.

2.1. Seismic Impact Model

In this forward model, it is assumed that individual grains of diameter D each impact the river bed with speed w_i , assumed normal to the bed, where w_i depends on D and other fluvial parameters, as will be discussed in Section 2.2. For a single particle, the impact force can be described by an elastic contact problem, of which the simplest case is perfectly elastic Hertzian contact [Johnson, 1987]. For this case, the maximum force amplitude F_0 and time of contact Δt are given by well known expressions [Johnson, 1987]. For $D < 2 \text{ m}$, $w_i > 0.1 \text{ m/s}$, and a typical elastic modulus ($E = 5 \cdot 10^{10} \text{ Pa}$), then $\Delta t \lesssim 10^{-3} \text{ s}$, and the impact can be assumed to be instantaneous relative to the frequency range of interest, and impart an impulse equal to

$$I \approx \frac{2}{\pi} F_0 \Delta t \approx 2mw_i, \quad (1)$$

where $m = \rho_s V_p$ is the mass of the particle, V_p is the particle volume, and ρ_s is rock density. If the impact is not perfectly elastic, I could be as much as a factor of 2 smaller (when perfectly inelastic), in which case $I \approx mw_i$. A force history for a single particle's instantaneous impulse can then be expressed as $F_1(t) = I\delta(t)$ where $\delta(t)$ is the Dirac delta function.

Given a force history $F(t)$ at location \mathbf{x}_0 , the ground velocity $\dot{u}(t)$ at location \mathbf{x} is given in the frequency domain by

$$\dot{u}(f, \mathbf{x}) = 2\pi i f F(f, \mathbf{x}_0) G(f, \mathbf{x}; \mathbf{x}_0) \quad (2)$$

where $F(f) \equiv \mathcal{F}[F(t)]$ is the Fourier transform of $F(t)$, and $G(t)$ is the displacement Green's function. Since w_i is vertically

¹Seismological Laboratory, California Institute of Technology, Pasadena, California, USA.

²Division of Geological and Planetary Sciences, California Institute of Technology, Pasadena, California, USA.

incident, Rayleigh waves are expected to be the dominant waves excited [e.g., *Sanchez-Sesma et al.*, 2011]. For a horizontally homogeneous medium, and assuming an approximate Rayleigh-wave sensitivity that decays with depth proportional to e^{-kz} , we can follow *Aki and Richards* [2002] and approximate the amplitude of the Rayleigh-wave Green's function as

$$|G(f, \mathbf{x}; \mathbf{x}_0)| \approx \frac{k}{8\rho_s v_c v_u} \sqrt{\frac{2}{\pi k r}} e^{-\pi f r / (v_u Q)}, \quad (3)$$

where v_c is the Rayleigh-wave phase velocity, v_u is group velocity, $k \equiv 2\pi f / v_c$ is the angular wavenumber, $r \equiv |\mathbf{x} - \mathbf{x}_0|$ is the source-station distance, and Q is the (dimensionless) quality factor.

To use Eq. (3), we must have estimates of the frequency-dependent v_c , v_u and Q . For v_c and v_u , we use values of average shear wave speed for a typical generic rock site (and in the frequency range of interest) given as

$$v_s = v_0 (z/z_0)^\alpha, \quad (4)$$

where $v_0 = 2206$ m/s, $z_0 = 1000$ m, and $\alpha = 0.272$ [*Boore and Joyner*, 1997]. Using these values, and approximations as above, one can solve for v_c as

$$v_c = v_{c0} (f/f_0)^{-\xi}, \quad (5)$$

where $v_{c0} = [(2\pi z_0 f_0)^{-\alpha} v_0 \Gamma(1+\alpha)]^{1/(1-\alpha)}$, $\xi = \alpha/(1-\alpha)$, and $\Gamma(x)$ is the gamma function (see Supplementary Material). With values as given above, $v_{c0} = 1295$ m/s, $f_0 = 1$ Hz, $\xi = 0.374$. Furthermore, under the same approximations, it can be shown that $v_u = v_c/(1+\xi) = 0.73v_c$. On the other hand, Q is typically assumed to be of the form of $Q = Q_0(f/f_0)^\eta$ [e.g., *Erickson et al.*, 2004]. *Anderson and Hough* [1984] suggest that for the relatively high frequencies and shallow depths of interest, $Q_0 \approx 20$ and $\eta = 0$ are reasonable approximations, and we use these values throughout, despite known spatial variations in Q [e.g., *Campbell*, 2009].

To describe the rate of impacts, we define $n(D)$ to be the number of particles with grain size D , per unit length of river per unit D . If the average time between impacts of each particle is $t_i(D)$, then $\int_D n \cdot t_i^{-1} dD$ is the total rate of impacts per unit length of river. In Section 2.2, we relate n/t_i to sediment flux.

In the simplest version of the model, we assume that all impacts occur randomly spaced in time, i.e. $F(t) = I \sum_j^N \delta(t - t_j)$, with random t_j , and N being the number of impacts. For random t_j , one can show that $F(f) = F_1(f) \sqrt{N} \equiv I \sqrt{N}$, so that the sum of impacts does not affect the shape of the force spectrum, and the force amplitude squared grows linearly with N . We can now express the power spectral density (PSD) of a station's velocity time series (per unit grain size D) to be

$$P_v(f; D) = \int_R \frac{n}{t_i} |\dot{u}_1(f)|^2 d\mathbf{x}_0, \quad (6)$$

where the integral is along the full length of river R , and $\dot{u}_1(t)$ is the ground velocity due to $F_1(t)$.

In order to approximate Eq. (6) analytically, we assume an infinitely long and straight river whose closest point is r_0 from the seismic station (see Fig. 1a). Substituting $F_1(f)$, Eq. (1) and Eq. (3) into Eq. (2) we arrive at

$$P_v(f; D) \approx \frac{n}{t_i} \frac{\pi^2 f^3 m^2 w_i^2}{\rho_s^2 v_s^2 v_u^2} \chi(\beta), \quad (7)$$

where

$$\chi(\beta) \equiv \int_{-\infty}^{\infty} \frac{1}{\sqrt{1+y^2}} e^{-\beta \sqrt{1+y^2}} dy \quad (8)$$

and $\beta \equiv 2\pi r_0 (1+\xi) f^{1+\xi-\eta} / (v_{c0} Q_0 f_0^{\xi-\eta})$ are dimensionless. As shown in the Supplementary Material, $\chi(\beta)$ can be approximated

as

$$\chi(\beta) \approx 2 \log \left(1 + \frac{1}{\beta} \right) e^{-2\beta} + (1 - e^{-\beta}) e^{-\beta} \sqrt{\frac{2\pi}{\beta}}. \quad (9)$$

It may be noted that Eq. (7) scales with frequency roughly as $f^{4.9} \exp[-2\pi r_0 f^{1.4} / (Q_0 v_{c0} f_0^{0.4})]$.

Finally, the total PSD, $P_v^T(f)$, is given as an integral over the grain size distribution

$$P_v^T(f) = \int_D P_v(f; D) dD. \quad (10)$$

Using Eq. (9) in Eq. (7) and substituting into Eq. (10) then yields an algebraic expression for the total PSD, $P_v^T(f)$, as a function of frequency f , grain size distribution and other model parameters.

The random impact model discussed above can be made more realistic by including the correlated impacts of the same particle. If N_c hops of a single particle occur before the impact time becomes significantly different from an integer multiple of the timescale between impacts, t_i , then the forcing

$$F_{N_c}(t) \equiv I \sum_{j=0}^{N_c-1} \delta(t - jt_i) \quad (11)$$

can be used instead of $F_1(t)$ to approximate an average over timescale $N_c t_i$. This then results in a frequency modulation of Eq. (7) equivalent to multiplying Eq. (7) by

$$T(f) \equiv \frac{|\sum_{j=0}^{N_c-1} e^{-2\pi i j t_i f}|^2}{N_c} = \frac{|1 + e^{-2\pi i t_i f} + \dots|^2}{N_c}. \quad (12)$$

Since there is expected to be a large variance in hop times [e.g., *Lamb et al.*, 2008a], N_c is likely a relatively small number, i.e. $N_c \lesssim 4$, and therefore only has a second-order effect on the model (see Section 3).

2.2. Fluvial Components

To drive the seismic model, relationships are needed to predict the rate and velocity of streambed impacts by fluvially transported particles. Here we follow recent work that characterized these processes in the context of bedrock incision [e.g., *Sklar and Dietrich*, 2004; *Turowski et al.*, 2007; *Lamb et al.*, 2008a]; in particular, we use the model of *Lamb et al.* [2008a] because it explicitly solves for particle fall velocity. Owing to the strong dependency of seismic energy on particle size and impact velocity (i.e., Eq. (7) scales as $m^2 w_i^2$), we focus on seismic energy generated from saltating particles alone and neglect particles that are rolling or sliding along the bed, particles suspended in the flow, and viscous damping of particles impacts by the fluid [cf. *Lamb et al.*, 2008a]. The rate of particle impacts per unit channel length (for a given grain size) can be calculated from

$$\frac{n}{t_i} = \frac{C_1 W q_{bD} \bar{w}_s}{V_p U_b H_b} \quad (13)$$

where W is the average channel-bed width, q_{bD} is the volumetric sediment flux per unit grain size D per unit channel width traveling as bedload, U_b is the vertically-averaged streamwise particle velocity and H_b is the bedload layer height, \bar{w}_s is the depth-averaged particle settling velocity, and V_p is the particle volume. $C_1 \approx 2/3$ accounts for the fact that the total time between impacts should also include the particle ejection or rise time as well as the fall time [*Sklar and Dietrich*, 2004].

The depth-averaged bedload velocity and layer height are given as empirical expressions by *Sklar and Dietrich* [2004] derived from several different bedload studies. The best fit relationships are

$$U_b = 1.56 \sqrt{RgD} \left(\frac{\tau_*}{\tau_{*c}} \right)^{0.56}, U_b \leq U \quad (14)$$

and

$$H_b = 1.44D \left(\frac{\tau_*}{\tau_{*c}} \right)^{0.50}, \quad H_b \leq H \quad (15)$$

where $R = (\rho_s - \rho_f)/\rho_f$, $\rho_s \approx 2700 \text{ kg/m}^3$ and $\rho_f = 1000 \text{ kg/m}^3$ are the sediment and fluid densities, respectively, $g = 9.8 \text{ m/s}^2$ is the acceleration due to gravity, $\tau_* \equiv u_*^2/(RgD)$, u_* is the bed shear velocity, and H is the total flow depth. U is the depth-averaged flow velocity calculated as $U = 8.1u_*(H/k_s)^{1/6}$ [Parker, 1991], where $k_s = 3D_{50}$ [e.g., Kamphuis, 1974], and the critical value of the Shields stress (τ_{*c}) is the value of τ_* at the threshold of particle motion found from Lamb *et al.* [2008b] for the median grain size D_{50} . For other grain sizes, we calculate $\tau_{*c} = \tau_{*c50}(D/D_{50})^{-\gamma}$, where $\gamma \approx 0.9$ [Parker, 1990]. The bed shear velocity is calculated assuming steady and uniform flow as $u_* = \sqrt{gH \sin \theta}$, where θ is the channel-bed slope angle.

The particle impact velocity normal to the bed can be calculated from a balance between the forces of gravity and drag for spherical particles [Lamb *et al.*, 2008a] as

$$w_i(H_b) = w_{st} \cos \theta \sqrt{1 - \exp[-\hat{H}_b]}, \quad (16)$$

where $w_{st} = \sqrt{4RgD/(3C_d)}$ is the terminal settling velocity, and $\hat{H}_b \equiv 3C_d \rho_f H_b / (2\rho_s D \cos \theta)$. The drag coefficient C_d depends on the particle Reynolds number and grain shape, and we calculate C_d from the empirical formula of Dietrich [1982] for natural sediment (Corey Shape Factor = 0.8, Powers Roundness Scale = 3.5) (for $0.01 \text{ m} < D < 0.6 \text{ m}$, C_d ranges from 1.4 to 0.5). The average settling velocity through the bedload layer can be calculated from the same force balance as above

$$\bar{w}_s = \frac{H_b}{\int_0^{H_b} w_i(z)^{-1} dz} = \frac{\hat{H}_b w_{st} \cos \theta}{2 \log[e^{\hat{H}_b/2} + \sqrt{e^{\hat{H}_b} - 1}]} \quad (17)$$

Finally, the average time between impacts for a given saltating particle can be calculated from Sklar and Dietrich [2004] as

$$t_i = \frac{H_b}{C_1 \bar{w}_s} \quad (18)$$

In bedrock rivers, bedload flux q_{bD} is determined by the supply of sediment from neighboring hillslopes and from upstream, and is the primary fluvial parameter that we attempt to constrain. However, with ample supply, the total flux $q_b \equiv \int q_{bD} dD$ is limited by the river's transport capacity q_{bc} , which can be calculated following Fernandez Luque and van Beek [1976] as

$$q_{bc} = 5.7 \sqrt{RgD_{50}^3 (\tau_* - \tau_{*c})^{3/2}} \quad (19)$$

3. Model Results

Although our model is meant to be general, it is useful to explore the model results using parameters that scale roughly after a natural river. Herein we use the Trisuli River, which is one of the main trans-Himalayan rivers in central Nepal. Burtin *et al.* [2008] attributed heightened seismic noise to sediment transport in a $\approx 25 \text{ km}$ reach of the Trisuli River that is steep ($\theta \approx 1.4^\circ$), relatively narrow ($W \lesssim 50 \text{ m}$), and rapidly incising (5 mm/yr) into the underlying bedrock [Lavé and Avouac, 2001]. Although water discharge was not measured locally, water depth was measured $\approx 50 \text{ km}$ downstream [Burtin *et al.*, 2008], from which we derive water depth at the location of interest using standard hydraulic geometry formulations (see Supplementary Material). We assume sediment to be spherical ($V_p = \pi D^3/6$) and estimate sediment size from grain size measurements of Attal and Lavé [2006] for a reach of the nearby Marsyandi River with a similar drainage area and slope (see Supplementary Material).

The final model is produced when Eq. (13) for n/t_i and Eq. (16) for w_i are substituted into Eq. (7) along with the given expressions

for U_b , H_b and \bar{w}_s . Eq. (7) then predicts the observed seismic PSD (P_v) for a given D , H , θ , W , r_0 , and q_{bD} . Before showing model results, we observe that once all expressions are substituted, Eq. (7) approximately scales as $D^3 q_{bD}$ for $\hat{H}_b \lesssim 1$ and constant τ_*/τ_{*c} . This implies that the seismic signal is strongly dependent on D , and that one must have good constraints on grain size distribution if q_b is to be inferred from observations of P_v . Note that the fluvial parameterizations for n/t_i and w_i may be different than assumed here in rivers with large scale bedrock roughness where oblique bed impacts may cause impact velocities to scale with flow velocity U rather than settling velocity w_{st} [e.g., Johnson and Whipple, 2010]. If true, this would cause Eq. (7) to scale approximately with D^2 rather than D^3 , and non-vertical impact would also cause a higher fraction of Love waves to be generated than assumed.

Using representative values from Lavé and Avouac [2001], Attal and Lavé [2006] and Burtin *et al.* [2008], we obtain PSDs as function of frequency f as shown in Fig. 1 for 2 choices of r_0 and 3 choices of D . In these plots, it is assumed that all particles are of median size $D = D_{50}$ and that $q_b = q_{bD}$ describes the flux of these particles. We predict the general spectral features of such PSDs to be similar for any steady impact model where the frequencies of interest are less than one over the impact time (i.e., $f < 1/\Delta t$). As shown, the modification introduced by Eq. (12) creates a modulation in the PSDs with frequency spacing $\Delta f = 1/t_i$, revealing a potential seismic signature of sediment size independent of sediment flux, but has no effect on a smoothed version of the PSDs. Compared with the PSDs in Figure 6 of Burtin *et al.* [2008], the model is able to predict some aspects of the observations, including the general peak around $\approx 7 \text{ Hz}$, the sharper increase of the PSDs to this peak compared to the more gradual decrease at higher frequencies, and the higher PSD values at high frequencies (up to 15-20 Hz) for stations that are closer to the Trisuli River. The modulation introduced by Eq. (12) may also be observed by Burtin *et al.* [2008], and could potentially be used as a constraint on the grain size distribution.

To explore the dependence of Eq. (7) on fluvial parameters, in Fig. 2 we plot P_v for fixed $r_0 = 600 \text{ m}$ at $f = 7 \text{ Hz}$ (near the peak of the PSD) but with variable H , θ , D and q_b . For fixed q_b the PSDs have the somewhat unintuitive feature that they decrease both with increasing slope (θ) and with increasing flow depth (H) (solid lines of Fig. 2a). This results from a larger hop height and velocity, which reduces the impact rate (Eq. (13)) in the fluvial framework used. However, q_b may increase with both θ and H ; for example, if we set $q_b = q_{bc}$ then the PSDs increase with both θ and H (dashed lines of Fig. 2a).

So far, expressions have been evaluated and plotted for a single grain size, D . As noted above, the approximate D^3 dependence of P_v implies that larger grain sizes have a disproportionately larger effect on the seismic signal compared to smaller grain sizes. For comparisons with observations, then, it is important to use a grain size distribution that is realistic. Thus, instead of using a typical log-normal distribution of grain sizes, which has an unrealistically long tail at large D , we introduce a new log-'raised cosine' distribution, which has almost the same shape as a log-normal distribution but has a cut-off at both large and small D (see Fig. 3a). The raised cosine distribution is defined by

$$\hat{p}(x; \mu, s) = \frac{1}{2s} \left[1 + \cos \pi \left(\frac{x - \mu}{s} \right) \right], \quad -s < x - \mu < s \quad (20)$$

and $\hat{p}(x; \mu, s) = 0$ otherwise, and has equivalent mean, median, and variance as a normal distribution $N(\mu, \sigma_g^2)$ if we choose $s \equiv \sigma_g / \sqrt{1/3 - 2/\pi^2}$ (where μ and σ_g are the mean and standard deviation of the normal distribution). To best fit the data for Attal and Lavé [2006] for the region of interest, we choose

$D_{50} = 0.15$ m and $\sigma_g = 0.52$ (dimensionless, see Supplementary Material). The resulting log-‘raised cosine’ distribution $p(D) \equiv \hat{p}(\log[D]; \log[D_{50}], s)/D$ as well as the P_v resulting from this grain size distribution are plotted in Fig. 3a. For this example, the peak in P_v occurs at $D = 0.34$ m and corresponds to D_{94} , the 94th percentile grain size. Integrating P_v over all D results in the total PSD, which in this case is $P_v^T = -150.3$ dB. While we expect σ_g to be realistic, in Fig. 3b, we show the sensitivity of the dominant grain size to variations in σ_g . As shown, the dominant grain size is typically far above the median grain size D_{50} except when σ_g is unrealistically small (< 0.3).

Finally, we make a preliminary attempt at inverting the observations of Burtin *et al.* [2008] for the total bedload flux q_b , without attempting to calibrate the model, and assuming the average estimated and measured fluvial and seismic parameters as before. As stated previously, this inversion relies heavily on adequate knowledge of grain size distribution, which is lacking, and despite other poorly constrained parameters, this is likely the cause of the largest uncertainty. Given the scaling of P_v with $D^3 q_{bD} \equiv D^3 p q_b$, and the dominant D being close to D_{94} , if the grain size distribution changes with flow discharge through the monsoon season then the seismic PSD approximately constrains $D_{94}^3 q_b$ rather than q_b alone. It is also unknown what fraction of the observed seismic noise may be attributable to water flow noise (or other environmental sources), but a large portion of the seismic signal is likely due to bedload [Burtin *et al.*, 2008]. Assuming the grain size distribution is unchanging (as given above), and assuming the full seismic signal is due to bedload, q_b as inverted from the seismic data (see Fig. 3c) seems to scale approximately with $q_{bc}/5$ but has the clear hysteresis inherent in the Burtin *et al.* [2008] data. The predicted hysteresis in sediment flux as a function of discharge is supported by measurements of Gabet *et al.* [2008] in a neighboring river, and likely occurs as sediment supply from hillslopes is depleted near the end of the wet season. These observations are consistent with a supply-limited river, where $q_b < q_{bc}$ (Fig. 3c), resulting in bedrock that is partially exposed [Sklar and Dietrich, 2004] and susceptible to rapid erosion [Lavé and Avouac, 2001]. The calculations presented show the feasibility of such an inversion and we expect the framework described here to be useful to constrain sediment flux from seismic observations at other rivers.

Acknowledgments. The authors thank J.-P. Avouac, L. Bollinger, and J. Lavé for helpful comments, and thank J. Johnson and L. Sklar for thoughtful reviews. This research was partially supported by NSF grant EAR0922199 to MPL. [Accepted 12/28/11]

References

- Aki, K., and P. G. Richards (2002), *Quantitative Seismology*, second ed., 700 pp., University Science Books, Sausalito.
- Anderson, J. G., and S. E. Hough (1984), A model for the shape of the Fourier amplitude spectrum of acceleration at high frequencies, *Bull. Seismol. Soc. Am.*, **74**, 1969–1993.
- Attal, M., and J. Lavé (2006), Changes of bedload characteristics along the Marsyandi River (central Nepal): Implications for understanding hillslope sediment supply, sediment load evolution along fluvial networks, and denudation in active orogenic belts, in *Tectonics, Climate, and Landscape Evolution: Special Paper 398*, edited by S. D. Willett, N. Hovius, M. T. Brandon, and D. Fisher, pp. 143–171, Geological Society of America.
- Barton, J. S., R. L. Slingerland, S. Pittman, and T. B. Gabrielson (2006), Passive acoustic monitoring of coarse bedload transport on the Trinity River, in *Eighth Federal Interagency Sedimentation Conference*, pp. 627–634, Reno, NV.
- Boore, D. M., and W. B. Joyner (1997), Site amplification for generic rock sites, *Bull. Seismol. Soc. Am.*, **87**, 327–341.
- Burtin, A., L. Bollinger, J. Vergne, R. Cattin, and J. L. Nabelek (2008), Spectral analysis of seismic noise induced by rivers: A new tool to monitor spatiotemporal changes in stream hydrodynamics, *J. Geophys. Res.*, **113**, B05301, doi:10.1029/2007JB005034.
- Burtin, A., J. Vergne, L. Rivera, and P. Dubernet (2010), Location of river-induced seismic signal from noise correlation functions, *Geophys. J. Int.*, **182**, 1161–1173.
- Burtin, A., R. Cattin, L. Bollinger, J. Vergne, P. Steer, A. Robert, N. Findling, and C. Tiberi (2011), Towards the hydrologic and bed load monitoring from high-frequency seismic noise in a braided river: The ‘torrent de St Pierre’, French Alps, *J. Hydrol.*, **408**, 43–53.
- Campbell, K. W. (2009), Estimates of shear-wave Q and κ_0 for unconsolidated and semiconsolidated sediments in eastern North America, *Bull. Seismol. Soc. Am.*, **99**, 2365–2392.
- Dietrich, W. E. (1982), Settling velocity of natural particles, *Water Resour. Res.*, **18**, 1615–1626.
- Erickson, D., D. E. McNamara, and H. M. Benz (2004), Frequency-dependent Lg Q within the continental United States, *Bull. Seismol. Soc. Am.*, **94**, 1630–1643.
- Fernandez Luque, F. R., and R. van Beek (1976), Erosion and transport of bed-load sediment, *J. Hydraul. Res.*, **14**, 127–144.
- Gabet, E. J., D. W. Burbank, B. Pratt-Sitaula, J. Putkonen, and B. Bookhagen (2008), Modern erosion rates in the high Himalayas of Nepal, *Earth Planet. Sci. Lett.*, **267**, 482–494.
- Govi, M., F. Maraga, and F. Moia (1993), Seismic detectors for continuous bed load monitoring in a gravel stream, *Hydrolog. Sci. J.*, **38**, 123–132.
- Hsu, L., N. J. Finnegan, and E. E. Brodsky (2011), A seismic signature of river bedload transport during storm events, *Geophys. Res. Lett.*, **38**, L13407, doi:10.1029/2011GL047759.
- Johnson, J. P., and K. X. Whipple (2010), Evaluating the controls of shear stress, sediment supply, alluvial cover, and channel morphology on experimental bedrock incision rate, *J. Geophys. Res.*, **115**, F02018, doi:10.1029/2009JF001335.
- Johnson, K. L. (1987), *Contact Mechanics*, 452 pp., Cambridge University Press., New York.
- Kamphuis, J. W. (1974), Determination of sand roughness for fixed beds, *J. Hydraul. Res.*, **12**, 193–203.
- Lamb, M. P., W. E. Dietrich, and L. S. Sklar (2008a), A model for fluvial bedrock incision by impacting suspended and bed load sediment, *J. Geophys. Res.*, **113**, F03025, doi:10.1029/2007JF000915.
- Lamb, M. P., W. E. Dietrich, and J. G. Venditti (2008b), Is the critical Shields stress for incipient sediment motion dependent on channel-bed slope?, *J. Geophys. Res.*, **113**, F02008, doi:10.1029/2007JF000813.
- Lavé, J., and J. P. Avouac (2001), Fluvial incision and tectonic uplift across the Himalayas of central Nepal, *J. Geophys. Res.*, **106**, 26,561–26,591.
- Parker, G. (1990), Surface-based bedload transport relation for gravel rivers, *J. Hydraul. Res.*, **28**, 417–436.
- Parker, G. (1991), Selective sorting and abrasion of river gravel. ii: Applications, *J. Hydraul. Eng.*, **117**, 150–151.
- Sanchez-Sesma, F. J., R. L. Weaver, H. Kawase, S. Matsushima, F. Luzon, and M. Campillo (2011), Energy partitions among elastic waves for dynamic surface loads in a semi-infinite solid, *Bull. Seismol. Soc. Am.*, **101**, 1704–1709.
- Sklar, L. S., and W. E. Dietrich (2004), A mechanistic model for river incision into bedrock by saltating bed load, *Water Resour. Res.*, **40**, W06301, doi:10.1029/2003WR002496.
- Turowski, J. M., D. Lague, and N. Hovius (2007), Cover effect in bedrock abrasion: A new derivation and its implications for the modeling of bedrock channel morphology, *J. Geophys. Res.*, **112**, F04006, doi:10.1029/2006JF000697.
- Whipple, K. X. (2004), Bedrock rivers and the geomorphology of active orogens, *Ann. Rev. Earth Pl. Sc.*, **32**, 151–185.

V. C. Tsai, Seismological Laboratory, MS 252-21, California Institute of Technology, 1200 E. California Blvd., Pasadena, CA 91125, USA. (tsai@caltech.edu)

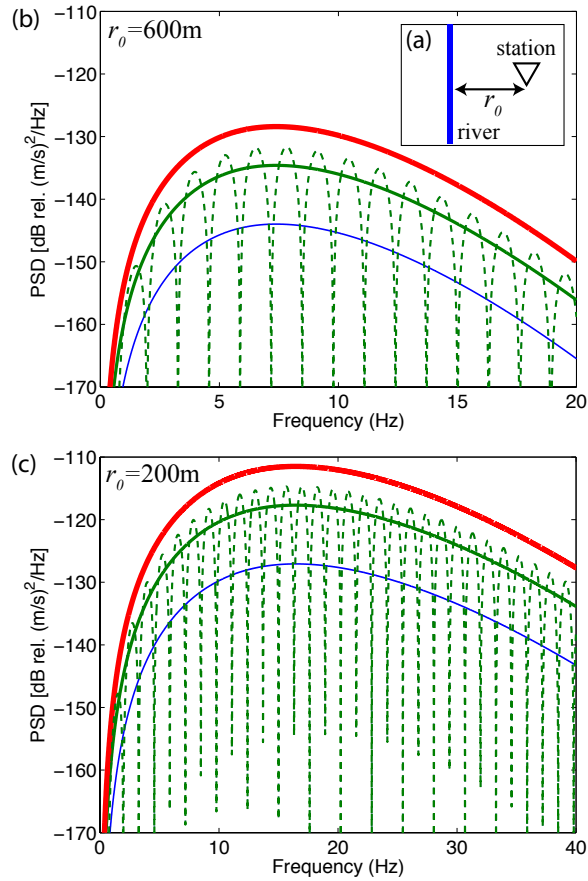


Figure 1. PSD as a function of f for 3 different choices of D . Using $H = 4$ m, $\theta = 1.4^\circ$, $q_b = 10^{-3}$ m²/s, $W = 50$ m, and for $D = 0.3$ m (thin blue), 0.5 m (medium green), 0.7 m (thick red); dashed green line is for $D = 0.5$ m but uses the modification of Eq. (12) with $N_c = 2$. Inset (a) Schematic of idealized river and seismic station geometry, defining r_0 , the distance of the station from the river. (b) $r_0 = 600$ m. (c) $r_0 = 200$ m. All PSDs are given in decibels (dB) relative to velocity power ($10 \log_{10} P_v$). Note that the peaks in the PSDs occur at higher frequencies for closer stations because higher frequency seismic energy is preferentially attenuated with distance.

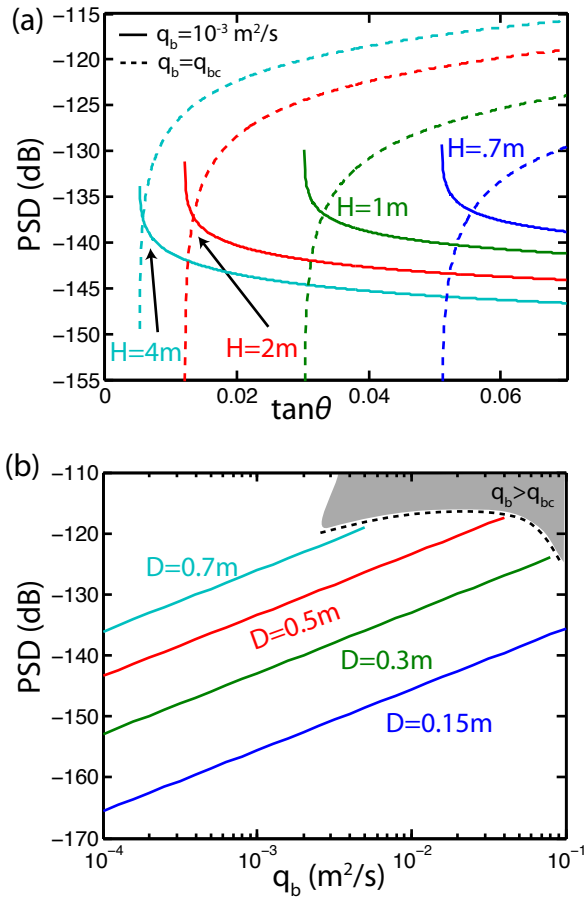


Figure 2. (a) PSD vs. $S = \tan \theta$. (b) PSD vs. q_b . Both panels use $W = 50 \text{ m}$, $r_0 = 600 \text{ m}$, $f = 7 \text{ Hz}$. Panel (a) uses $D = 0.3 \text{ m}$, and is plotted for 4 different values of $H = 0.7 \text{ m}$ (blue), 1.0 m (green), 2.0 m (red), and 4.0 m (cyan). Solid lines use $q_b = 0.001 \text{ m}^2/\text{s}$ whereas dashed lines use $q_b = q_{bc}$. Panel (b) uses $H = 3 \text{ m}$, $\theta = 1.4^\circ$ ($\tan \theta = 0.024$), and is plotted for 4 different values of $D = 0.15 \text{ m}$ (blue), 0.3 m (green), 0.5 m (red), and 0.7 m (cyan). Gray area in panel (b) denotes approximately where $q_b > q_{bc}$, which cannot be achieved.

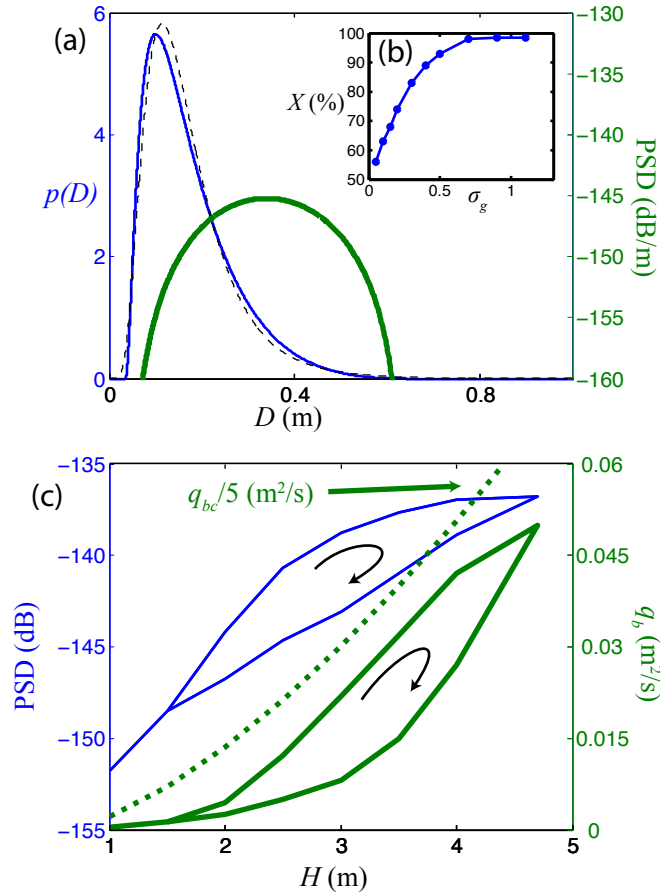


Figure 3. Sensitivity of PSD to grain size, and inversion of PSD data for q_b . (a) Log-'raised cosine' grain size probability distribution (thin blue) and resulting PSD (thick green) for $D_{50} = 0.15$ m, $\sigma_g = 0.52$, $H = 4$ m, $\theta = 1.4^\circ$, and total $q_b = 10^{-3}$ m^2/s . For comparison, a log-normal distribution with the same D_{50} and geometric standard deviation σ_g (dimensionless) is also plotted (dashed black). Inset (b) Grain size percentile X where D_X yields the largest PSD, as a function of σ_g . (c) Prediction of q_b from fitting PSD data. The thin blue curve is the approximate PSD (P_v^T) of Burtin *et al.* [2008] for station H0460 averaged over $3 < f < 15$ Hz. The thick green solid curve is the q_b needed to achieve this average P_v^T , assuming a grain size distribution as in Fig. 3, and $r_0 = 600$ m. The green dashed curve is $q_b/5$.

Supplementary Material for ‘A Physical Model for Seismic Noise Generation from Sediment Transport in Rivers’

Victor C. Tsai, Brent Minchew, Michael P. Lamb, and Jean-Paul Ampuero

1 Evaluation of Phase Velocity

With shear wave speed as given in Eq. (4) of the main text as $v_s = v_0(z/z_0)^\alpha$, and assuming Rayleigh-wave sensitivity that decays with depth proportional to e^{-kz} , then the Rayleigh-wave phase velocity can be approximately expressed as

$$v_c \approx \frac{\int_0^\infty v_s(z)e^{-kz}dz}{\int_0^\infty e^{-kz}dz} = \frac{kv_0}{z_0^\alpha} \int_0^\infty z^\alpha e^{-kz}dz = \frac{v_0\Gamma(1+\alpha)}{z_0^\alpha k^\alpha}. \quad (1)$$

Substituting $k = 2\pi f/v_c$, one can then solve for v_c as

$$v_c = \left[\frac{v_0\Gamma(1+\alpha)}{z_0^\alpha (2\pi f)^\alpha} \right]^{1/(1-\alpha)} = \left[\frac{v_0\Gamma(1+\alpha)}{(2\pi z_0 f_0)^\alpha} \right]^{1/(1-\alpha)} \left[\frac{f}{f_0} \right]^{-\alpha/(1-\alpha)} \quad (2)$$

2 Approximation of $\chi(\beta)$

$\chi(\beta)$ is defined in Eq. (8) of the main text as

$$\chi(\beta) \equiv \int_{-\infty}^{\infty} \frac{1}{\sqrt{1+s^2}} e^{-\beta\sqrt{1+s^2}} ds. \quad (3)$$

To approximately evaluate this integral, we consider the limits $\beta \ll 1$ and $\beta \gg 1$. For $\beta \ll 1$, $\chi(\beta)$ can be approximated as

$$\chi(\beta) \approx 2 \int_0^1 \frac{1}{\sqrt{1+s^2}} ds + 2 \int_1^\infty \frac{1}{s} e^{-\beta s} ds = 2 \sinh^{-1} 1 + 2\Gamma(0, \beta), \quad (4)$$

where $\Gamma(0, \beta)$ is the incomplete gamma function. $\Gamma(0, \beta)$ can be approximated as $\Gamma(0, \beta) \approx e^{-\beta} \log(1 + 1/\beta)$. For $\beta \ll 1$, $\Gamma(0, \beta) \gg \sinh^{-1} 1$, so we finally have

$$\chi(\beta) \approx 2e^{-\beta} \log(1 + 1/\beta), \beta \ll 1. \quad (5)$$

On the other hand, when $\beta \gg 1$, $\chi(\beta)$ can be approximated as

$$\chi(\beta) \approx 2 \int_0^\infty e^{-\beta(1+s^2/2)} ds = e^{-\beta} \sqrt{\frac{2\pi}{\beta}}, \beta \gg 1. \quad (6)$$

Smoothly transitioning between Eq. (5) and (6) with an exponential weighting then results in

$$\chi(\beta) \approx 2 \log \left(1 + \frac{1}{\beta} \right) e^{-2\beta} + (1 - e^{-\beta}) e^{-\beta} \sqrt{\frac{2\pi}{\beta}}. \quad (7)$$

3 Estimation of Local Water Depth

For given slope S , channel width W , and channel depth H , the total water flux $Q = WHU$, where average velocity U is given in the main text and can be written as $U \propto H^{2/3} S^{1/2}$ so that $Q \propto WH^{5/3} S^{1/2}$. Thus,

$$H_2 = H_1 \left(\frac{Q_2 W_1 S_1^{1/2}}{Q_1 W_2 S_2^{1/2}} \right)^{3/5}, \quad (8)$$

where subscripts refer to different locations. Since W and S can be estimated from imagery, and *Lave and Avouac* [2001] provide estimates of Q along the Trisuli, we can estimate H_2 near the seismic stations of interest relative to the H measured in the town of Betrawati. Our estimates are that $Q_2/Q_1 \approx 800\text{m}^3/\text{s}/1000\text{m}^3/\text{s} \approx 0.8$, $W_2/W_1 \approx 35\text{m}/70\text{m} \approx 0.5$, and $S_2/S_1 \approx 0.025/0.010 \approx 2.5$ so that $H_2 \approx 1.0H_1$. This means that the water level records at Betrawati can be used, without modification, as estimates of the water levels near the seismic stations of interest.

4 Estimation of Grain Size Distribution

To estimate the grain size distribution of the Trisuli River close to the seismic stations of interest, we assume that the distribution is similar to that of the

nearby Marsyandi River at a location with similar drainage area and slope. Based on the descriptions of the two rivers in Plate 6 of *Lave and Avouac* [2001], we find that a location just north of the main central thrust (MCT) along the Marsyandi has similar slope (2.5°) and $Q_{10} \approx 10^3 \text{ m}^3/\text{s}$ as the region of the Trisuli of interest, and we choose this location as representative. *Attal and Lave* [2006] provide average grain size distributions on the Marsyandi both upstream and downstream of the MCT, so we take an average of these two zones as representative. For this average, the distribution of grain sizes larger than 5 cm is approximately 17%, 38%, 39%, 6% and 0% in bins of 5-8 cm, 8-16 cm, 16-32 cm, 32-64 cm, and > 64 cm, respectively. Performing a best-fit to these data using the log-‘raised cosine’ distribution discussed in the main text, we obtain a median grain size $D_{50} = 0.15$ m and an equivalent normal standard deviation of $\sigma_g = 0.525$ (i.e., $s = 1.45$). This best-fitting model results in a grain size distribution of 12%, 42%, 38%, 8% and 0% for the same grain size bins.

As stated in the main text, we choose to use the log-‘raised cosine’ distribution rather than the more commonly used log-normal distribution because the log-normal distribution has an unrealistically long tail at large (and small) grain sizes. Since our model is quite sensitive to the largest grain sizes (with an approximate D^3 dependence of P_v), having a realistic tail at the high end of the grain size distribution is therefore important for the model prediction. To provide a sense for how different the log-‘raised cosine’ and log-normal distributions are, we note that the log-normal distribution plotted in Fig. 3a of the main text has a grain size distribution with 10%, 43%, 38%, 7% and 0.3% in the same grain size bins described above. Thus, while the distributions are very similar (and fit the measured grain size distribution nearly equally as well), the 0.3% at very large grain sizes (> 64 cm) would result in significant seismic power predicted for those grains (from the sensitivity of the model to large grain sizes) despite the very small percentage, and would therefore bias our prediction somewhat. For any model (like the one presented here) that is sensitive to the tails of a grain size distribution that is known to be bounded, we recommend use of the log-‘raised cosine’ over the log-normal distribution.